

000
001
002054
055
056

Multi-channel Weighted Nuclear Norm Minimization for Real Color Image Denoising

057
058
059003
004
005
006
007060
061
062
063

Anonymous ICCV submission

008
009
010
011
012064
065
066
067
068

Paper ID 572

013
014
015069
070
071

Abstract

016
017
018
019
020
021
022
023
024
025
026
027
028
029
030
031
032
033
034
035
036
037072
073
074
075
076
077
078
079
080
081
082
083
084
085
086
087
088
089
090
091
092
093
094
095
096
097
098
099
100
101
102
103
104
105
106
107

The noise structures among the R, G, B channels of real images are quite different due to the preprocessing steps, such as demosaicing, white balance, etc., of the in-camera imaging pipelines. This makes the real image denoising problem much more complex than traditional grayscale image denoising. In this paper, we propose a multi-channel optimization model for real color image denoising. Specifically, we introduce a weighting matrix into the data term to process adaptively each part of R, G, B channels in the joint patches concatenated by corresponding patches in these channels. In the regularization term, we employ the weighted nuclear norm to exploit the non-local self similar property. The proposed multi-channel weighted nuclear norm minimization (WNNM) model is much more complex than the standard WNNM model. We reformulate the proposed model into a linear constrained optimization problem and solve it by the alternating direction method of multipliers algorithm. Each alternative updating step has closed-form solution and the convergence results are given. Experiments on benchmark datasets demonstrate that the proposed model outperforms state-of-the-art denoising methods on synthetic as well as real-world noisy images.

038
039
040

1. Introduction

041
042
043
044
045
046
047
048
049
050
051
052
053

Image denoising is an important problem in enhancing the image quality in computer vision systems. The traditional grayscale image denoising problem aims to recover the clean image \mathbf{x} from the noisy observation $\mathbf{y} = \mathbf{x} + \mathbf{n}$, where \mathbf{n} is often assumed to be additive white Gaussian noise (AWGN). Most image denoising methods in this field either employ the non-local self similarity (NSS) of natural images [1–7] or learn generative or discriminative denoisers from paired natural clean images and synthetic noisy images [8–12]. Among these methods, the weighted nuclear norm minimization (WNNM) method achieves excellent denoising performance by exploiting the NSS property

via low rank regularization.

The real color image denoising problem is not a trivial extension from single channel (grayscale image) to multiple channels (color image). The reason is that the noise structures are quite different among the R, G, B channels of images captured by CCD or CMOS cameras due to the on-board processing steps [13]. This makes the real color image denoising problem much more complex. Directly applying the denoising methods for grayscale images to each channel of color images separately would obtain bad performance [14]. There are several work [14–19] proposed specifically for color image denoising. The method [15] first transforms the color images into the luminance/chrominance space such as YCbCr before denoising, but this would make the noise distribution more complex in color images. The methods of [14, 19] process the joint patches concatenated by the corresponding patches in R, G, B channels and treat equally the patches in different channels. This would generate false colors or artifacts [14]. The methods of [16–18] ignore the non-local self similarity property of natural images, and their performance would be largely depressed [2, 7].

In order to deal with the R, G, B channels in color images more effectively, different noise properties of different channels should be considered in solving real color image denoising problem. Besides, due to its expressive denoising performance, the WNNM model [7] is employed to exploit the NSS property of natural images. In this paper, we proposed a multi-channel WNNM model for real color image denoising. By introducing a weighting matrix to the WNNM model, the proposed multi-channel WNNM model no longer has closed-form solutions and more challenging to solve. By reformulating the proposed multi-channel WNNM model into a linear constrained program with two variables, the relaxed problem can be solved under the alternating direction method of multipliers (ADMM) [20] framework. Each variable can be updated with closed-form solution [7, 21]. We also give the convergency results with detailed proof to guarantee a rational termination of the proposed algorithm.

108

2. Related Work

109

2.1. Weighted Nuclear Norm Minimization

111

As an extension to the nuclear norm minimization (NNM) model [22], the weighted nuclear norm minimization (WNNM) model [7] is described as

$$\min_{\mathbf{X}} \|\mathbf{Y} - \mathbf{X}\|_F^2 + \|\mathbf{X}\|_{w,*} \quad (1)$$

115

where $\|\mathbf{X}\|_{w,*} = \sum_i w_i \sigma_i(\mathbf{X})$ is the weighted nuclear norm of matrix \mathbf{X} , and $w = [w_1, \dots, w_n]^\top$, $w_i \geq 0$ is the weight vector, $\sigma_i(\mathbf{X})$ is the i -th singular value of matrix \mathbf{X} . According to the Corollary 1 of [23], the problem (1) has closed-form solution if the weights are non-decreasing

$$\hat{\mathbf{X}} = \mathbf{U} \mathcal{S}_{w/2}(\Sigma) \mathbf{V}^\top \quad (2)$$

121

where $\mathbf{Y} = \mathbf{U} \Sigma \mathbf{V}^\top$ is the singular value decomposition [24] of \mathbf{Y} and $\mathcal{S}_\tau(\bullet)$ is the generalized soft-thresholding operator with weight vector w :

$$\mathcal{S}_{w/2}(\Sigma_{ii}) = \max(\Sigma_{ii} - w_{ii}/2, 0) \quad (3)$$

125

Though having achieved excellent performance on grayscale image denoising, the WNNM model would generate false colors or artifacts [14], if being directly extended to real color image denoising by processing each channel separately or joint vectors concatenated by multiple channels. In this paper, for real noisy image denoising, we propose a multi-channel WNNM model which preserve the power of WNNM and be able to process the differences among different channels.

135

2.2. Real Color Image Denoising

136

During the last decade, several denoising methods are proposed for real color image denoising [15–17, 19]. Among them, the CBM3D [15] first transform the RGB image into luminance-chrominance space (e.g., YCbCr) and then apply the famous BM3D method [2] on each channel separately with the patches being grouped only in the luminance channel. In [16], the authors proposed the “Noise Level Function” to estimate and remove the noise for each channel in natural images. However, the methods processing each channel separately would achieve inferior performance than processing jointly these channels [14]. The methods of [17, 19, 25] perform real color image denoising by concatenating the patches in R, G, B channels into joint vectors. However, the concatenation would treat each channel equally and ignore the different noise properties among these channels. The method in [18] models the cross-channel noise in real noisy image as a multivariate Gaussian and the noise is removed by the Bayesian non-local means filter [26]. The commercial software Neat Image [27] estimates the noise parameters from a flat region of the given noisy image and filters the noise correspondingly. But these methods [18, 27] ignore the non-local self similarity property of natural images [2, 7].

160

In this paper, we introduce a weighting matrix which add different weights to different channels for color image

denoising. The proposed multi-channel method can effectively solve the problem of different noise structures among different channels.

162

163

164

165

166

167

168

169

170

171

172

173

174

175

176

177

178

179

180

181

182

183

184

185

186

187

188

189

190

191

192

193

194

195

196

197

198

199

200

201

202

203

204

205

206

207

208

209

210

211

212

213

214

215

where \mathbf{W} is the weighting matrix. For simplicity, we assume \mathbf{W} to be a diagonal matrix. Unfortunately, the proposed multi-channel WNNM problem cannot be solved in an analytical form. In [23], when the weights on singular values are non-descending, the weighted nuclear norm proximal operator can have global optimum with closed-form solution. However, such property is not valid for the multi-channel WNNM model. The reason is that the weighting matrix \mathbf{W} is added to the matrix \mathbf{X} instead of its singular values. Besides, the elements in \mathbf{W} is not in a non-descending order with respect to the singular value of \mathbf{X} . This makes the proposed model more difficult to optimize than the original WNNM model.

This can be solved by introducing an augmented variable \mathbf{Z} , and the above multi-channel WNNM problem is equivalent to a linearly constrained non-convex problem with two variables.

$$\min_{\mathbf{X}, \mathbf{Z}} \|\mathbf{W}(\mathbf{Y} - \mathbf{X})\|_F^2 + \|\mathbf{Z}\|_{w,*} \quad \text{s.t.} \quad \mathbf{X} = \mathbf{Z}. \quad (5)$$

This is an optimization problem with functions of two variables \mathbf{X} and \mathbf{Z} with linearly constrained condition of $\mathbf{X} = \mathbf{Z}$. In fact, this problem can be solved by the alternating direction method of multipliers (ADMM) algorithm, which will be introduced in the next subsection.

3.2. The Setting of Weights

Assume the matrix \mathbf{Y} containing the noisy patches in R, G, B channels as $\mathbf{Y} = [\mathbf{Y}_r^\top \mathbf{Y}_g^\top \mathbf{Y}_b^\top]^\top$, the corresponding clean matrix $\mathbf{X} = [\mathbf{X}_r^\top \mathbf{X}_g^\top \mathbf{X}_b^\top]^\top$, and the weights w for the singular values of \mathbf{X} , the setting of the weights in the weighting matrix \mathbf{W} can be automatically determined under

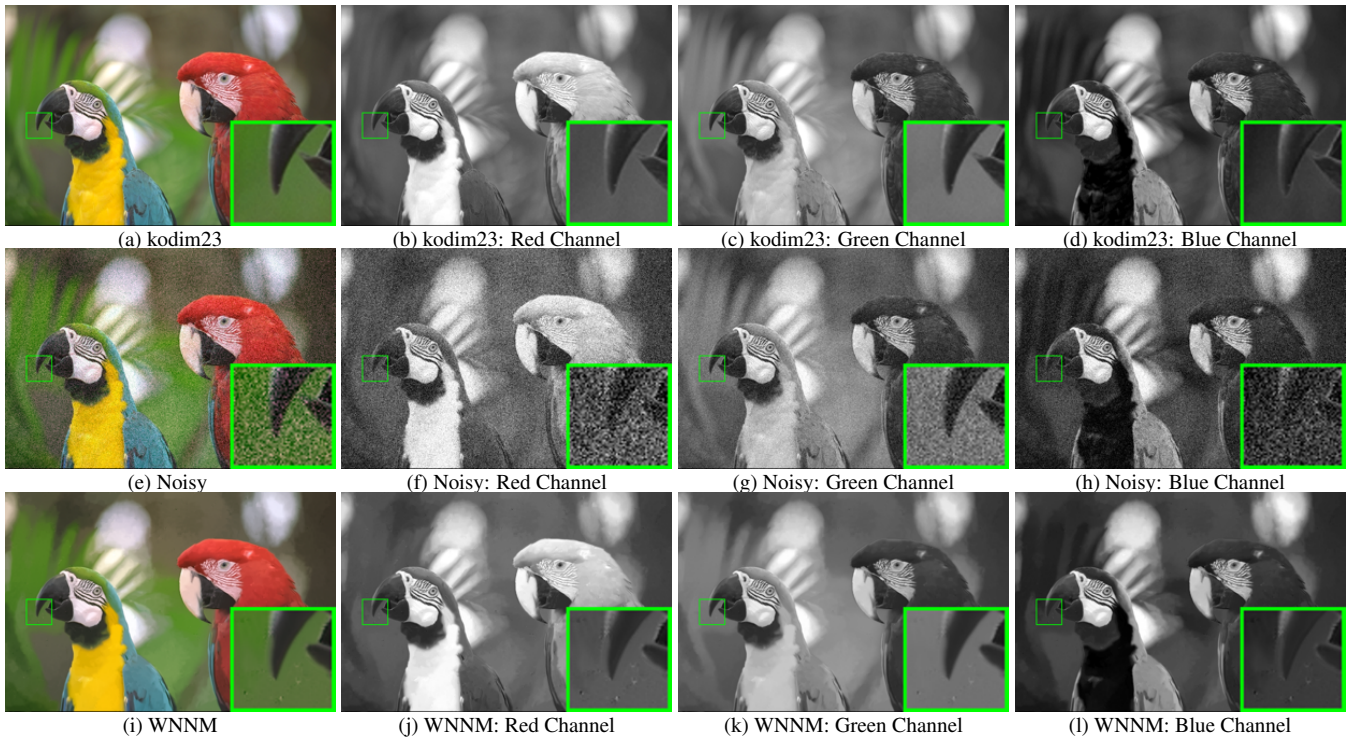


Figure 1. The image “kodim23” of the Kodak PhotoCD dataset, its degraded version, and the image recovered by WNNM. The R, G, B channels are also listed here for image quality comparison.

the Bayesian framework:

$$\begin{aligned}\hat{\mathbf{X}} &= \arg \max_{\mathbf{X}} \ln P(\mathbf{X}|\mathbf{Y}, \mathbf{w}) \\ &= \arg \max_{\mathbf{X}} \{\ln P(\mathbf{Y}|\mathbf{X}) + \ln P(\mathbf{X}|\mathbf{w})\}. \end{aligned}\quad (6)$$

The log-likelihood term $\ln P(\mathbf{Y}|\mathbf{X})$ is characterized by the statistics of noise, which is assumed to be channel-wise independent white Gaussian with standard deviations $\{\sigma_r, \sigma_g, \sigma_b\}$

$$P(\mathbf{Y}|\mathbf{X}) = \prod_{c \in \{r, g, b\}} (2\pi\sigma_c^2)^{-\frac{3p^2}{2}} \exp\left(-\frac{1}{2\sigma_c^2} \|\mathbf{Y}_c - \mathbf{X}_c\|_F^2\right). \quad (7)$$

We assume that the matrix \mathbf{X} follows the following distribution

$$P(\mathbf{X}|\mathbf{w}) \propto \exp\left(-\frac{1}{2} \|\mathbf{X}\|_{\mathbf{w},*}\right). \quad (8)$$

Putting (8) and (7) into (6), we have

$$\hat{\mathbf{X}} = \arg \min_{\mathbf{X}} \|\mathbf{W}(\mathbf{Y} - \mathbf{X})\|_F^2 + \|\mathbf{X}\|_{\mathbf{w},*}, \quad (9)$$

where

$$\mathbf{W} = \begin{pmatrix} \sigma_r^{-2} \mathbf{I} & \mathbf{0} & \mathbf{0} \\ \mathbf{0} & \sigma_g^{-2} \mathbf{I} & \mathbf{0} \\ \mathbf{0} & \mathbf{0} & \sigma_b^{-2} \mathbf{I} \end{pmatrix}. \quad (10)$$

3.3. Optimization

To solve the above optimization problem, we first derive its augmented Lagrangian function as

$$\begin{aligned}\mathcal{L}(\mathbf{X}, \mathbf{Z}, \mathbf{A}, \rho) &= \|\mathbf{W}(\mathbf{Y} - \mathbf{X})\|_F^2 + \|\mathbf{Z}\|_{\mathbf{w},*} \\ &\quad + \langle \mathbf{A}, \mathbf{X} - \mathbf{Z} \rangle + \frac{\rho}{2} \|\mathbf{X} - \mathbf{Z}\|_F^2 \end{aligned}\quad (11)$$

where \mathbf{A} is the augmented Lagrangian multiplier and $\rho > 0$ is the penalty parameter. After some simple calculations, we can obtain the following equivalent form of the Lagrangian function

$$\begin{aligned}\mathcal{L}(\mathbf{X}, \mathbf{Z}, \mathbf{A}, \rho) &= \|\mathbf{W}(\mathbf{Y} - \mathbf{X})\|_F^2 + \|\mathbf{Z}\|_{\mathbf{w},*} \\ &\quad + \frac{\rho}{2} \|\mathbf{X} - \mathbf{Z} + \rho^{-1} \mathbf{A}\|_F^2 \end{aligned}\quad (12)$$

We initialize the matrix variables \mathbf{X}_0 , \mathbf{Z}_0 , and \mathbf{A}_0 to be zero matrix of suitable size. Taking derivative of the Lagrangian function \mathcal{L} with respect to the variables \mathbf{X} and \mathbf{Z} and setting the derivative function to be zero, we can alternatively update the iterations of the ADMM algorithm as follows:

(1) Update \mathbf{X} while fixing \mathbf{Z} and \mathbf{A} :

$$\mathbf{X}_{k+1} = \arg \min_{\mathbf{X}} \|\mathbf{WY} - \mathbf{WX}\|_F^2 + \frac{\rho_k}{2} \|\mathbf{X} - \mathbf{Z}_k + \rho_k^{-1} \mathbf{A}_k\|_F^2 \quad (13)$$

324 This is a mixed weighted least square and standard least
 325 square problem and we could derive its closed-form solution:
 326
 327

$$\mathbf{X}_{k+1} = (\mathbf{W}^\top \mathbf{W} + \frac{\rho_k}{2} \mathbf{I})^{-1} (\mathbf{W}^\top \mathbf{W} \mathbf{Y} + \frac{\rho_k}{2} \mathbf{Z}_k - \frac{1}{2} \mathbf{A}_k) \quad (14)$$

(2) Update \mathbf{Z} while fixing \mathbf{X} and \mathbf{A} :

$$\mathbf{Z}_{k+1} = \arg \min_{\mathbf{Z}} \frac{\rho_k}{2} \|\mathbf{Z} - (\mathbf{X}_{k+1} + \rho_k^{-1} \mathbf{A}_k)\|_F^2 + \|\mathbf{Z}\|_{w,*} \quad (15)$$

335 According to the Theorem 1 in [23], given the $\mathbf{X}_{k+1} + \rho_k^{-1} \mathbf{A}_k = \mathbf{U}_k \boldsymbol{\Sigma}_k \mathbf{V}_k^\top$ be the SVD of $\mathbf{X}_{k+1} + \rho_k^{-1} \mathbf{A}_k$,
 336 where $\boldsymbol{\Sigma}_k = \begin{pmatrix} \text{diag}(\sigma_1, \sigma_2, \dots, \sigma_n) \\ \mathbf{0} \end{pmatrix} \in \mathbb{R}^{m \times n}$, then the
 337 global optimum of the above problem is $\hat{\mathbf{Z}} = \mathbf{U}_k \hat{\boldsymbol{\Sigma}}_k \mathbf{V}_k^\top$,
 338 where $\hat{\boldsymbol{\Sigma}}_k = \begin{pmatrix} \text{diag}(\hat{\sigma}_1, \hat{\sigma}_2, \dots, \hat{\sigma}_n) \\ \mathbf{0} \end{pmatrix} \in \mathbb{R}^{m \times n}$ and
 339 $(\hat{\sigma}_1, \hat{\sigma}_2, \dots, \hat{\sigma}_n)$ is the solution to the following convex opti-
 340 mization problem:
 341
 342

$$\begin{aligned} \min_{\hat{\sigma}_1, \hat{\sigma}_2, \dots, \hat{\sigma}_n} & \sum_{i=1}^n (\sigma_i - \hat{\sigma}_i)^2 + \frac{2w_i}{\rho_k} \hat{\sigma}_i \\ \text{s.t. } & \hat{\sigma}_1 \geq \hat{\sigma}_2 \geq \dots \geq \hat{\sigma}_n \geq 0. \end{aligned} \quad (16)$$

According to the Remark 1 in [23], the problem above has closed-form solution

$$\hat{\sigma}_i = \begin{cases} 0 & \text{if } c_2 < 0 \\ \frac{c_1 + \sqrt{c_2}}{2} & \text{if } c_2 \geq 0 \end{cases} \quad (17)$$

where $c_1 = \sigma_i - \epsilon$, $c_2 = (\sigma_i - \epsilon)^2 - \frac{8C}{\rho_k}$ and C is set as $\sqrt{2n}$ by experience in image denoising.

(3) Update \mathbf{A} while fixing \mathbf{X} and \mathbf{Z} :

$$\mathbf{A}_{k+1} = \mathbf{A}_k + \rho_k (\mathbf{X}_{k+1} - \mathbf{Z}_{k+1}) \quad (18)$$

(4) Update ρ_k as $\rho_{k+1} = \mu * \rho_k$, where $\mu > 1$ is a .

The above 4 alternative updating steps are repeated until the convergence conditions are satisfied or the number of iterations exceeds a preset maximum number, e.g., K_1 . The overall algorithm will achieve its convergence conditions when $\|\mathbf{X}_{k+1} - \mathbf{Z}_{k+1}\|_F \leq \text{Tol}$, $\|\mathbf{X}_{k+1} - \mathbf{X}_k\|_F \leq \text{Tol}$, and $\|\mathbf{Z}_{k+1} - \mathbf{Z}_k\|_F \leq \text{Tol}$ are simultaneously satisfied, where $\text{Tol} > 0$ is a small tolerance. We summarize the optimization steps in Algorithm 1 (A1). We give a theorem, i.e., Theorem 1, to guarantee the convergence of the proposed Algorithm 1. Note that since the weighted nuclear norm is non-convex in general, we employ an unbounded sequence of $\{\rho_k\}$ here to make sure that the Algorithm 1 is convergent.

Theorem 1. Assume the weights in w are in a non-descending order, the sequence $\{\mathbf{X}_k\}$, $\{\mathbf{Z}_k\}$, and $\{\mathbf{A}_k\}$

A1: Solve Multi-channel WNNM via ADMM	378
Input: Matrices \mathbf{Y} and \mathbf{W} , $\mu > 1$, $\text{Tol} > 0$, $K_1 > 0$;	379
Initialization: $\mathbf{X}_0 = \mathbf{Z}_0 = \mathbf{A}_0 = \mathbf{0}$, $\rho_0 > 0$, $T = \text{False}$,	380
$k = 0$;	381
While ($T == \text{false}$) do	382
1. Update \mathbf{X}_{k+1} as	383
$\mathbf{X}_{k+1} = (\mathbf{W}^\top \mathbf{W} + \frac{\rho_k}{2} \mathbf{I})^{-1} (\mathbf{W}^\top \mathbf{W} \mathbf{Y} + \frac{\rho_k}{2} \mathbf{Z}_k - \frac{1}{2} \mathbf{A}_k)$	384
2. Update \mathbf{Z}_{k+1} by solving the WNNM problem	385
$\min_{\mathbf{Z}} \frac{\rho_k}{2} \ \mathbf{Z} - (\mathbf{X}_{k+1} + \rho_k^{-1} \mathbf{A}_k)\ _F^2 + \ \mathbf{Z}\ _{w,*}$	386
3. Update \mathbf{A}_{k+1} as $\mathbf{A}_{k+1} = \mathbf{A}_k + \rho_k (\mathbf{X}_{k+1} - \mathbf{Z}_{k+1})$	387
4. Update $\rho_{k+1} = \mu * \rho_k$;	388
5. $k \leftarrow k + 1$;	389
if ($\ \mathbf{X}_{k+1} - \mathbf{Z}_{k+1}\ _F / \ \mathbf{Z}_{k+1}\ _F < \text{Tol}$) or ($k \geq K_1$)	390
5. $T \leftarrow \text{True}$	391
end if	392
end while	393
Output: Matrices \mathbf{X} and \mathbf{Z} .	394

generated in Algorithm 1 satisfy:

$$(1) \lim_{k \rightarrow \infty} \|\mathbf{X}_{k+1} - \mathbf{Z}_{k+1}\|_F = 0; \quad (19)$$

$$(2) \lim_{k \rightarrow \infty} \|\mathbf{X}_{k+1} - \mathbf{X}_k\|_F = 0; \quad (20)$$

$$(3) \lim_{k \rightarrow \infty} \|\mathbf{Z}_{k+1} - \mathbf{Z}_k\|_F = 0. \quad (21)$$

Proof. We give proof sketch here and detailed proof of this theorem can be found in Appendix. We can first proof that the sequence $\{\mathbf{A}_k\}$ generated by Algorithm 1 is upper bounded. Since $\{\rho_k\}$ is unbounded, that is $\lim_{k \rightarrow \infty} \rho_k = +\infty$, we can proof that the sequence of Lagrangian function $\{\mathcal{L}(\mathbf{X}_{k+1}, \mathbf{Z}_{k+1}, \mathbf{A}_k, \rho_k)\}$ is also upper bounded. Hence, both $\{\mathbf{WY} - \mathbf{WX}_k\}$ and $\{\mathbf{Z}_k\}$ are upper bounded. According to Eq. (18), we can proof that $\lim_{k \rightarrow \infty} \|\mathbf{X}_{k+1} - \mathbf{Z}_{k+1}\|_F = \lim_{k \rightarrow \infty} \rho_k^{-1} \|\mathbf{A}_{k+1} - \mathbf{A}_k\|_F = 0$, and (1) is proofed. Then we can proof that $\lim_{k \rightarrow \infty} \|\mathbf{X}_{k+1} - \mathbf{X}_k\|_F \leq \lim_{k \rightarrow \infty} \|(\mathbf{W}^\top \mathbf{W} + \frac{\rho_k}{2} \mathbf{I})^{-1} (\mathbf{W}^\top \mathbf{W} \mathbf{Y} - \mathbf{W}^\top \mathbf{W} \mathbf{Z}_k - \frac{1}{2} \mathbf{A}_k)\|_F + \rho_k^{-1} \|\mathbf{A}_k - \mathbf{A}_{k-1}\|_F = 0$ and hence (2) is proofed. Then (3) can be proofed by checking that $\lim_{k \rightarrow \infty} \|\mathbf{Z}_{k+1} - \mathbf{Z}_k\|_F \leq \lim_{k \rightarrow \infty} \|\boldsymbol{\Sigma}_{k-1} - \mathcal{S}_{w/\rho_{k-1}}(\boldsymbol{\Sigma}_{k-1})\|_F + \|\mathbf{X}_{k+1} - \mathbf{X}_k\|_F + \rho_k^{-1} \|\mathbf{A}_{k-1} + \mathbf{A}_{k+1} - \mathbf{A}_k\|_F = 0$, where $\mathbf{U}_{k-1} \boldsymbol{\Sigma}_{k-1} \mathbf{V}_{k-1}^\top$ is the SVD of the matrix $\mathbf{X}_k + \rho_{k-1} \mathbf{A}_{k-1}$. The proof sketch of Theorem 1 is end. \square

4. Multi-channel WNNM for Color Image Denoising

In this section, we apply the proposed multi-channel WNNM model on color image denoising problem. The multi-channel WNNM model can make use of the non-local self similarity property of natural images while treating each channel adaptively. In real-world noisy images, the

noise are first emerged in the RAW data, i.e., color filter array (CFA). The major noise generated in real noisy images are due to the discrete nature of light and thermal agitation [], which can be modeled as Poisson and Gaussian distribution, respectively. Since the Poisson distribution can be approximately modeled by Gaussian distribution, the overall noise model in each channel of the color image could be Gaussian. Hence, in this work we still choose to deal with the RGB channels in color images. Besides, even though if the demosaicing of RAW image generate similar distribution in noise in different channels, the channel-wise scaling in white balance would definitely change the noise distribution in each channel. Thus, the noise in R, G, B channels are definitely different which can be described by different noise levels and structures. According to above analysis, color image denoising is to recover the latent clean image \mathbf{x} from the observed noisy version $\mathbf{y}_c = \mathbf{x}_c + \mathbf{n}_c$, where $c \in \{R, G, B\}$ represent the R, G, B channels in color images and \mathbf{n}_c is the noise in the c channel (assumed to be additive white Gaussian noise).

The patches in color image \mathbf{y} are of size $p \times p \times 3$. For each patch \mathbf{y}_j , we search its non-local similar patches in a large area and stack the similar patches column by column. The resulting matrix $\mathbf{Y}_j \in \mathbb{R}^{3p^2 \times n}$, where n is the number of similar patches. The corresponding matrices containing the clean patches and the channel-wise noise are defined as \mathbf{X}_j and \mathbf{N}_j , respectively. Since \mathbf{X}_j is made of similar patches, it should be a low rank matrix. And hence the multi-channel WNNM model proposed in this paper can be used here. Compared to the original single channel WNNM model [7] proposed for grayscale image denoising

$$\min_{\mathbf{X}_j} \|\mathbf{W}_j(\mathbf{Y}_j - \mathbf{X}_j)\|_F^2 + \|\mathbf{X}_j\|_{w,*}. \quad (22)$$

When the weighting matrix $\mathbf{W}_j = \frac{1}{\sigma_n^2} \mathbf{I}$, where $\mathbf{I} \in \mathbb{R}^{3p^2 \times 3p^2}$ is the identity matrix, the multi-channel WNNM model will reduce to the WNNM model as a special case. The design of WNNM model also motivate us to consider a similar design of the weighting matrix. In order to deal with color image denoising task, the weighting matrix \mathbf{W}_j should be modified to be suitable for multi-channel cases. In fact, for the color image denoising task, a holistic try of the weighting matrix \mathbf{W}_j could be

Here, for simplicity, we assume that the noise in different channels are independent to each other. The experimental results have already demonstrated that this simple assumption could already generate the best denoising performance on benchmark real noisy image dataset. In this paper, we did not consider the correlations of noise among different channels, which is the future work of our research line. The determination of the weight vector in weighted nuclear norm is the same as in the WNNM model [23]. We set the weight vector as $w_i^{k+1} = \frac{C}{|\sigma_i(\mathbf{X}_k)| + \epsilon}$.

A2: Color Image Denoising by Multi-channel WNNM	486
Input: Noisy image \mathbf{y} , noise levels $\{\sigma_r, \sigma_g, \sigma_b\}$;	487
Initialization: $\hat{\mathbf{x}}^{(0)} = \mathbf{y}$, $\mathbf{y}^{(0)} = \mathbf{y}$;	488
for $k = 1 : K_2$ do	489
1. Set $\mathbf{y}^{(k)} = \hat{\mathbf{x}}^{(k-1)}$;	490
2. Extracte local patches $\{\mathbf{y}_j\}_{j=1}^N$ from $\mathbf{y}^{(k)}$;	491
for each patch \mathbf{y}_j do	492
3. Search non-local similar patches \mathbf{Y}_j ;	493
4. Estimate \mathbf{X}_j by applying the Algorithm 1 to \mathbf{Y}_j ;	494
end for	495
5. Aggregate $\{\mathbf{X}_j\}_{j=1}^N$ to form the image $\hat{\mathbf{x}}^{(k)}$;	496
end for	497
Output: Denoised image $\hat{\mathbf{x}}^{K_2}$.	498

The multi-channel WNNM is applied to the non-local similar patches of each local patch in the noisy image \mathbf{y} . And then all the patches are aggregated together to form the final recovered image $\hat{\mathbf{y}}$. We also perform the denoising procedure for several (K_2) iterations to obtain better denoising results. In Algorithm 2 (A2), we summarizes the denoising steps of multi-channel WNNM model on color image denoising.

5. Experiments

We evaluate the proposed method on synthetic noisy images as well as real noisy images. The synthetic noisy images are generated by adding additive white Gaussian noise with known noise standard derivations $\sigma_r, \sigma_g, \sigma_b$ for the R, G, B channels, respectively. We compare the proposed method with other state-of-the-art denoising algorithms including CBM3D [2, 15], MLP [10], CSF [11], WNNM [7], TNRD [12], “Noise Clinic” [17, 25], and the commercial software Neat Image [27].

In order to take fully comparison with the original WNNM method, we extended the WNNM method [23] in three directions. The first is to apply the WNNM method on each channel separately and we still call this method “WNNM”. The second is to concatenate the corresponding patches in the R, G, B channels into a joint patch and perform denoising in a joint manner. We call this method “WNNM1”. Note that both “WNNM” and “WNNM1” have closed form solutions since they are directly extended from the original WNNM. The third is to set the weighting matrix \mathbf{W} in the proposed multi-channel WNNM model as $\mathbf{W} = \sigma_n^2 \mathbf{I}$. This is to more clearly validate the effectiveness of the weighting matrix by reducing the multi-channel WNNM model to its special case: the WNNM model solved by ADMM algorithm. We call this method “WNNM2”. We set the same parameters settings for the “WNNM2” method and the proposed multi-channel WNNM method (called “Proposed”). For fair comparison, for “WNNM”, the corresponding noise levels σ_c of the c ($c = r, g, b$) channel

540
541
542
543
544
545
546
547
is input as known parameter; for “WNNM1”, we input the
noise level as $\sigma = \sqrt{(\sigma_r^2 + \sigma_g^2 + \sigma_b^2)/3}$ and tune the other
parameters to achieve its best denoising performance (i.e.,
highest average PSNR results); for “WNNM2”, we employ
the same parameter settings as the proposed multi-channel
WNNM method, which will be introduced in details in the
following sections.

548 549 5.1. Experiments on Synthetic Noisy Images

550 In this section, we compare the proposed method with
551 other competing method [7, 10–12, 15, 17, 27] on 24 high
552 quality color images from the Kodak PhotoCD Dataset
(<http://r0k.us/graphics/kodak/>), which are
553 shown in Fig. 1. Then we add additive white Gaussian
554 noise with different standard deviations to different chan-
555 nels of the color images. The standard deviations of noise
556 we add to the R, G, B channels of the 24 clean images are
557 40, 20, 30, respectively. We set the patch size as $p = 6$, the
558 number of non-local similar patches as $n = 70$, the win-
559 dows size for searching similar patches as $W = 20$. For
560 the proposed multi-channel WNNM model, we set the reg-
561 ularization parameter as $\lambda = 4$, the penalty parameter as
562 $\rho = 6$, the $\mu = 1.1$, the number of iterations in Algorithm
563 1 as $K_1 = 10$, the number of iterations in Algorithm 2 as
564 $K_2 = 8$.

565 We perform quantitative comparison on the 24 high qual-
566 ity images from the Kodak PhotoCD Dataset, which are
567 widely used for color image denoising task. The PSNR re-
568 sults of CBM3D [2], MLP [10], TNRD [12], NC [17, 25],
569 NI [27], “WNNMCW” [23], “WNNMJ”, “WNNMJadmm”
570 and the proposed multi-channel WNNM methods are listed
571 in Table 1. The best PSNR results of each image are
572 highlighted in bold. One can see that on all the 24 im-
573 ages, our method achieves the best PSNR values. On av-
574 erage, our proposed method has 0.45dB PSNR improve-
575 ments over the second best method, i.e., “WNNMJ” and
576 much higher PSNR gains over other competing methods.
577 Fig. 5 shows the denoised images of a scene in the Ko-
578 dak PhotoCD Dataset . We can see that CBM3D, NC, and
579 NI would either remain noise or generate artifacts, while
580 MLP, TNRD “WNNMCW”, “WNNMJ”, “WNNMJadmm”
581 over-smooth much the image. By using the proposed multi-
582 channel WNNM model, our method preserves the structures
583 (e.g., edges and textures) better across the R, G, B channels
584 and generate less artifacts than other denoising methods,
585 leading to visually pleasant outputs. More visual compari-
586 sons can be found in the supplementary file.

587 588 5.2. Experiments on Real Noisy Images

589 In the second part, we compare the proposed method
590 with other competing methods on the 15 real noisy images, ,
591 which are shown in Fig. 2, with “ground truth” clean images
592 [18]. The noisy images were collected under controlled in-



593 Figure 2. The 24 high quality color images from the Kodak Photo-
594 toCD Dataset.

595 door environment. Each scene was shot 500 times under the
596 same camera and camera setting. The mean image of the
597 500 shots is roughly taken as the “ground truth”, with which
598 the PSNR can be computed. Since the image size is very
599 large (about 7000×5000) and the scenes of this dataset
600 share repetitive contents, the authors of [18] cropped 15
601 smaller images (of size 512×512) to perform experiments.
602 In this section, we do not compare with the “WNNMCW”
603 method due to its inferior performance.

604 We firstly perform quantitative comparison on the 15
605 cropped images used in [18]. The PSNR results of CBM3D
606 [2], WNNM [7], MLP [10], TNRD [12], NC [17, 25], NI
607 [27] and CC [18] are listed in Table 2 (The results of CC
608 are copied from the original paper [18]). The best and sec-
609 ond best PSNR results of each image are highlighted in red
610 and blue, respectively. One can see that on 9 out of the 15
611 images, our method achieves the best PSNR values. CC
612 achieves the best PSNR on 3 of the 15 images. It should
613 be noted that in the CC method, a specific model is trained
614 for each camera and camera setting, while our method uses
615 the same model for all images. On average, our proposed
616 method has 0.28dB PSNR improvements over [18] and
617 much higher PSNR gains over other competing methods.
618 Fig. 5 shows the denoised images of a scene captured by
619 Canon 5D Mark 3 at ISO = 3200. We can see that CBM3D,
620 WNNM, NC, NI and CC would either remain noise or
621 generate artifacts, while MLP, TNRD over-smooth much
622 the image. By using the proposed multi-channel WNNM
623 model, our method preserves the structures (e.g., edges and
624 textures) better across the R, G, B channels and generate
625 less artifacts than other denoising methods, leading to vi-
626 sually pleasant outputs. More visual comparisons can be
627 found in the supplementary file.

6. Conclusion and Future Work

628 Most existing color image denoising methods treat the
629 R, G, B channels equally and ignore the different noise
630 structures in different channels. Common strategies that
631 processing each channel separately and concatenating the
632 RGB values into joint vectors would generate false color
633 or artifacts. In this paper, we proposed a novel model for
634

Table 1. PSNR(dB) results of different denoising algorithms on 20 natural images.

Image#	CBM3D	MLP	TNRD	Noise Clinic	Neat Image	WNNM	WNNM1	WNNM2	Proposed
1	25.24	25.70	25.74	24.90	23.85	26.01	25.95		26.66
2	28.27	30.12	30.21	25.87	25.90	30.08	30.11		30.20
3	28.81	31.19	31.49	28.58	26.00	31.58	31.61		32.25
4	27.95	29.88	29.86	25.67	25.82	30.13	30.16		30.49
5	25.03	26.00	26.18	25.15	24.38	26.44	26.39		26.82
6	26.24	26.84	26.90	24.74	24.65	27.39	27.30		27.98
7	27.88	30.28	30.40	27.69	25.63	30.47	30.54		30.98
8	25.05	25.59	25.83	25.30	24.02	26.71	26.75		26.90
9	28.44	30.75	30.81	27.44	25.94	30.86	30.92		31.49
10	28.27	30.38	30.57	28.42	25.87	30.65	30.68		31.26
11	26.95	28.00	28.14	24.67	25.32	28.19	28.16		28.63
12	28.76	30.87	31.05	28.37	26.01	30.97	31.06		31.48
13	23.76	23.95	23.99	22.76	23.53	24.27	24.15		24.89
14	26.02	26.97	27.11	25.68	24.94	27.20	27.15		27.57
15	28.38	30.15	30.44	28.21	26.06	30.52	30.60		30.81
16	27.75	28.82	28.87	26.66	25.69	29.27	29.21		29.96
17	27.90	29.57	29.80	28.32	25.85	29.78	29.79		30.40
18	25.77	26.40	26.41	25.70	24.74	26.63	26.56		27.22
19	27.30	28.67	28.81	26.52	25.40	29.19	29.22		29.57
20	28.96	30.40	30.76	25.90	24.95	30.79	30.83		31.07
21	26.54	27.53	27.60	26.48	25.06	27.80	27.75		28.34
22	27.05	28.17	28.27	26.60	25.36	28.21	28.16		28.64
23	29.14	32.31	32.51	23.24	26.13	31.89	31.97		32.34
24	25.75	26.41	26.53	25.73	24.55	27.10	27.03		27.59
Average	27.13	28.54	28.68	26.19	25.24	28.84	28.83		29.31

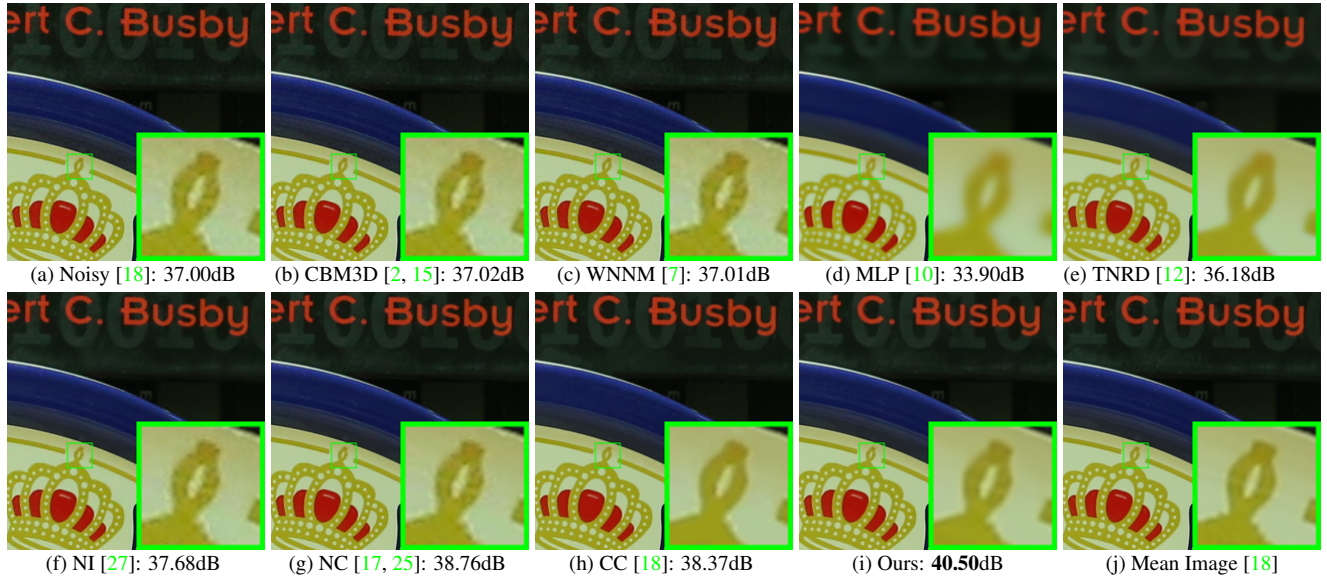


Figure 3. Denoised images of a region cropped from the real noisy image “Canon 5D Mark 3 ISO 3200 1” [18] by different methods. The images are better to be zoomed in on screen.

color image denoising which can explore the different noise structures among the R, G, B channels and exploit the non-local self similarity property of natural images. Specifically, we introduced a weighting matrix, which are employed to describe the noise levels of different channels, to the original weighted nuclear norm minimization (WNNM) model. Though the proposed model no longer has closed-form solution, we successfully solved the proposed model via the famous ADMM algorithm by introducing an addi-

tional variable with a linear constraint. The transformed problem has convergence property and can be solved in an alternative updating manner and both variables can be updated with closed-form solutions. We applied the proposed multi-channel WNNM model on color image denoising problem. Extensive experiments on benchmark datasets demonstrate that the proposed model outperforms the other competing denoising methods on both synthetic color noisy images as well as real-world noisy images. The introduce of

Table 2. PSNR(dB) results of different methods on 15 cropped real noisy images used in [18].

Camera Settings	CBM3D	MLP	TNRD	NI	NC	CC	WNNM1	WNNM2	Proposed
Canon 5D Mark III ISO = 3200	39.76	39.00	39.51	35.68	36.20	38.37	39.74	39.98	41.13
	36.40	36.34	36.47	34.03	34.35	35.37	35.12	36.65	37.28
	36.37	36.33	36.45	32.63	33.10	34.91	33.14	34.63	36.52
Nikon D600 ISO = 3200	34.18	34.70	34.79	31.78	32.28	34.98	35.08	35.08	35.53
	35.07	36.20	36.37	35.16	35.34	35.95	36.42	36.84	37.02
	37.13	39.33	39.49	39.98	40.51	41.15	40.78	39.24	39.56
Nikon D800 ISO = 1600	36.81	37.95	38.11	34.84	35.09	37.99	38.28	38.61	39.26
	37.76	40.23	40.52	38.42	38.65	40.36	41.24	40.81	41.43
	37.51	37.94	38.17	35.79	35.85	38.30	38.04	38.96	39.55
Nikon D800 ISO = 3200	35.05	37.55	37.69	38.36	38.56	39.01	39.93	37.97	38.91
	34.07	35.91	35.90	35.53	35.76	36.75	37.32	37.30	37.41
	34.42	38.15	38.21	40.05	40.59	39.06	41.52	38.68	39.39
Nikon D800 ISO = 6400	31.13	32.69	32.81	34.08	34.25	34.61	35.20	34.57	34.80
	31.22	32.33	32.33	32.13	32.38	33.21	33.61	33.43	33.95
	30.97	32.29	32.29	31.52	31.76	33.22	33.62	34.02	33.94
Average	35.19	36.46	36.61	35.33	35.65	36.88	37.27	37.12	37.71



Figure 4. The 15 cropped real noisy images used in [18].

the weighting matrix can indeed boost the performance of the original WNNM model on color image denoising. We believe that this work can be extended in at least three directions. Firstly, the proposed weighting matrix can be introduced into other methods designed for denoising grayscale images. Secondly, the weighting matrix beyond the diagonal form, such as correlation form [28], may bring better performance on color image denoising. Thirdly, the proposed multi-channel WNNM model can be further extended to deal with images with more channels, such as the hyperspectral images in remote sensing applications. We will focus our future work on these three directions.

7. A. Proof of Theorem 1.

Proof. 1. Firstly, we proof that the sequence $\{\mathbf{A}_k\}$ generated by Algorithm 1 is upper bounded. Let $\mathbf{X}_{k+1} + \rho_k^{-1}\mathbf{A}_k = \mathbf{U}_k\boldsymbol{\Sigma}_k\mathbf{V}_k^\top$ be its SVD in the $(k+1)$ -th iteration. According to Corollary 1 of [23], we can have the SVD of

\mathbf{Z}_{k+1} as $\mathbf{Z}_{k+1} = \mathbf{U}_k\hat{\boldsymbol{\Sigma}}_k\mathbf{V}_k^\top = \mathbf{U}_k\mathcal{S}_{\frac{w}{\rho_k}}(\boldsymbol{\Sigma}_k)\mathbf{V}_k^\top$. Then we have

$$\|\mathbf{A}_{k+1}\|_F = \|\mathbf{A}_k + \rho_k(\mathbf{X}_{k+1} - \mathbf{Z}_{k+1})\|_F \quad (23)$$

$$= \rho_k\|\rho_k^{-1}\mathbf{A}_k + \mathbf{X}_{k+1} - \mathbf{Z}_{k+1}\|_F \quad (24)$$

$$= \rho_k\|\mathbf{U}_k\boldsymbol{\Sigma}_k\mathbf{V}_k^\top - \mathbf{U}_k\mathcal{S}_{\frac{w}{\rho_k}}(\boldsymbol{\Sigma}_k)\mathbf{V}_k^\top\|_F \quad (25)$$

$$= \rho_k\|\boldsymbol{\Sigma}_k - \mathcal{S}_{\frac{w}{\rho_k}}(\boldsymbol{\Sigma}_k)\|_F \quad (26)$$

$$= \rho_k\sqrt{\sum_i(\boldsymbol{\Sigma}_k^{ii} - \mathcal{S}_{\frac{w_i}{\rho_k}}(\boldsymbol{\Sigma}_k^{ii}))^2} \quad (27)$$

$$\leq \rho_k\sqrt{\sum_i(\frac{w_i}{\rho_k})^2} = \sqrt{\sum_i w_i^2}. \quad (28)$$

The inequality above can be proofed as follows: given the diagonal matrix $\boldsymbol{\Sigma}_k$, we define $\boldsymbol{\Sigma}_k^{ii}$ as the i -th element of $\boldsymbol{\Sigma}_k^{ii}$. If $\boldsymbol{\Sigma}_k^{ii} \geq \frac{w_i}{\rho_k}$, we have $\mathcal{S}_{\frac{w_i}{\rho_k}}(\boldsymbol{\Sigma}_k^{ii}) = \boldsymbol{\Sigma}_k^{ii} - \frac{w_i}{\rho_k} \geq 0$. If $\boldsymbol{\Sigma}_k^{ii} < \frac{w_i}{\rho_k}$, we have $\mathcal{S}_{\frac{w_i}{\rho_k}}(\boldsymbol{\Sigma}_k^{ii}) = 0 < \boldsymbol{\Sigma}_k^{ii} + \frac{w_i}{\rho_k}$. After all, we have $|\boldsymbol{\Sigma}_k^{ii} - \mathcal{S}_{\frac{w_i}{\rho_k}}(\boldsymbol{\Sigma}_k^{ii})| \leq \frac{w_i}{\rho_k}$ and hence the inequality holds true. Hence, the sequence $\{\mathbf{A}_k\}$ is upper bounded.

2. Secondly, we proof that the sequence of Lagrangian function $\{\mathcal{L}(\mathbf{X}_{k+1}, \mathbf{Z}_{k+1}, \mathbf{A}_k, \rho_k)\}$ is also upper bounded. Since the global optimal solution of \mathbf{X} and \mathbf{Z} in corresponding subproblems, we always have $\mathcal{L}(\mathbf{X}_{k+1}, \mathbf{Z}_{k+1}, \mathbf{A}_k, \rho_k) \leq \mathcal{L}(\mathbf{X}_k, \mathbf{Z}_k, \mathbf{A}_k, \rho_k)$. Based on the updating rule that $\mathbf{A}_{k+1} = \mathbf{A}_k + \rho_k(\mathbf{X}_{k+1} - \mathbf{Z}_{k+1})$, we have $\mathcal{L}(\mathbf{X}_{k+1}, \mathbf{Z}_{k+1}, \mathbf{A}_{k+1}, \rho_{k+1}) = \mathcal{L}(\mathbf{X}_{k+1}, \mathbf{Z}_{k+1}, \mathbf{A}_k, \rho_k) + \langle \mathbf{A}_{k+1} - \mathbf{A}_k, \mathbf{X}_{k+1} - \mathbf{Z}_{k+1} \rangle + \frac{\rho_{k+1} - \rho_k}{2}\|\mathbf{X}_{k+1} - \mathbf{Z}_{k+1}\|_F^2 = \mathcal{L}(\mathbf{X}_{k+1}, \mathbf{Z}_{k+1}, \mathbf{A}_k, \rho_k) + \frac{\rho_{k+1} + \rho_k}{2\|\mathbf{A}_{k+1} - \mathbf{A}_k\|_F^2}$. Since

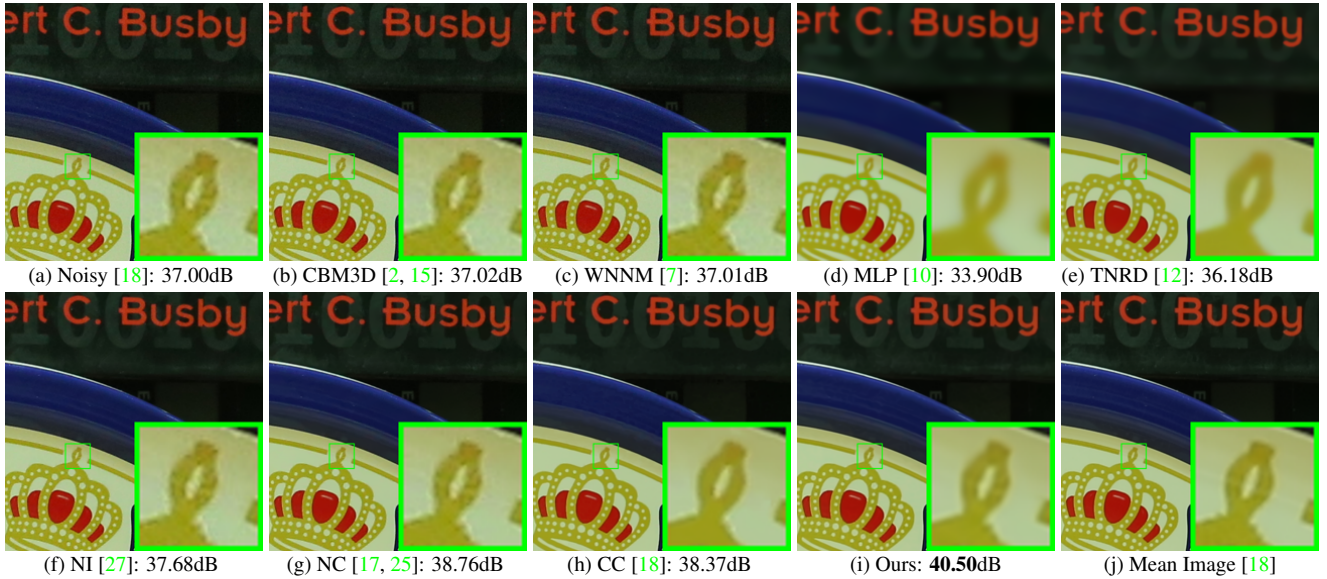


Figure 5. Denoised images of a region cropped from the real noisy image “Canon 5D Mark 3 ISO 3200 1” [18] by different methods. The images are better to be zoomed in on screen.

the sequence $\{\|\mathbf{A}_k\|\}$ is upper bounded, the sequence $\{\|\mathbf{A}_{k+1} - \mathbf{A}_k\|_F\}$ is also upper bounded. Denote by a the upper bound of $\{\|\mathbf{A}_{k+1} - \mathbf{A}_k\|_F\}$, we have $\mathcal{L}(\mathbf{X}_{k+1}, \mathbf{Z}_{k+1}, \mathbf{A}_{k+1}, \rho_{k+1}) \leq \mathcal{L}(\mathbf{X}_1, \mathbf{Z}_1, \mathbf{A}_0, \rho_0) + a \sum_{k=0}^{\infty} \frac{\rho_{k+1} + \rho_k}{2\rho_k^2} = \mathcal{L}(\mathbf{X}_1, \mathbf{Z}_1, \mathbf{A}_0, \rho_0) + a \sum_{k=0}^{\infty} \frac{\mu+1}{2\mu^k \rho_0} \leq \mathcal{L}(\mathbf{X}_1, \mathbf{Z}_1, \mathbf{A}_0, \rho_0) + \frac{a}{\rho_0} \sum_{k=0}^{\infty} \frac{1}{\mu^{k-1}}$. The last inequality holds since $\mu + 1 < 2\mu$. Since $\sum_{k=0}^{\infty} \frac{1}{\mu^{k-1}} < \infty$, the sequence of Lagrangian function $\mathcal{L}(\mathbf{X}_{k+1}, \mathbf{Z}_{k+1}, \mathbf{A}_{k+1}, \rho_{k+1})$ is upper bound.

3. Thirdly, we proof that the sequences of $\{\mathbf{X}_k\}$ and $\{\mathbf{Z}_k\}$ are upper bounded. Since $\|\mathbf{W}(\mathbf{Y} - \mathbf{X})\|_F^2 + \|\mathbf{Z}\|_{w,*} = \mathcal{L}(\mathbf{X}_k, \mathbf{Z}_k, \mathbf{A}_{k-1}, \rho_{k-1}) - \langle \mathbf{A}_k, \mathbf{X}_k - \mathbf{Z}_k \rangle - \frac{\rho_k}{2} \|\mathbf{X}_k - \mathbf{Z}_k\|_F^2 = \mathcal{L}(\mathbf{X}_k, \mathbf{Z}_k, \mathbf{A}_{k-1}, \rho_{k-1}) + \frac{1}{2\rho_k} (\|\mathbf{A}_{k-1}\|_F^2 - \|\mathbf{A}_k\|_F^2)$. Thus $\{\mathbf{W}(\mathbf{Y} - \mathbf{X}_k)\}$ and $\{\mathbf{Z}_k\}$ are upper bounded, and hence the sequence $\{\mathbf{X}_k\}$ is bounded by Cauchy-Schwarz inequality and triangle inequality. We can obtain that $\lim_{k \rightarrow \infty} \|\mathbf{X}_{k+1} - \mathbf{Z}_{k+1}\|_F = \lim_{k \rightarrow \infty} \rho_k^{-1} \|\mathbf{A}_{k+1} - \mathbf{A}_k\|_F = 0$ and the equation (1) is proofed.

4. Then we can proof that $\lim_{k \rightarrow \infty} \|\mathbf{X}_{k+1} - \mathbf{X}_k\|_F = \lim_{k \rightarrow \infty} \|(\mathbf{W}^\top \mathbf{W} + \frac{\rho_k}{2} \mathbf{I})^{-1} (\mathbf{W}^\top \mathbf{W} \mathbf{Y} - \mathbf{W}^\top \mathbf{W} \mathbf{Z}_k - \frac{1}{2} \mathbf{A}_k) - \rho_k^{-1} (\mathbf{A}_k - \mathbf{A}_{k-1})\|_F \leq \lim_{k \rightarrow \infty} \|(\mathbf{W}^\top \mathbf{W} + \frac{\rho_k}{2} \mathbf{I})^{-1} (\mathbf{W}^\top \mathbf{W} \mathbf{Y} - \mathbf{W}^\top \mathbf{W} \mathbf{Z}_k - \frac{1}{2} \mathbf{A}_k)\|_F + \rho_k^{-1} \|\mathbf{A}_k - \mathbf{A}_{k-1}\|_F = 0$ and hence (2) is proofed.

5. Then (3) can be proofed by checking that $\lim_{k \rightarrow \infty} \|\mathbf{Z}_{k+1} - \mathbf{Z}_k\|_F = \lim_{k \rightarrow \infty} \|\mathbf{X}_k + \rho_k^{-1} \mathbf{A}_{k-1} - \mathbf{Z}_k + \mathbf{X}_{k+1} - \mathbf{X}_k + \rho_k^{-1} \mathbf{A}_{k-1} + \rho_k^{-1} \mathbf{A}_k - \rho_k^{-1} \mathbf{A}_{k+1}\|_F \leq \lim_{k \rightarrow \infty} \|\Sigma_{k-1} - \mathcal{S}_{w/\rho_{k-1}}(\Sigma_{k-1})\|_F + \|\mathbf{X}_{k+1} - \mathbf{X}_k\|_F + \rho_k^{-1} \|\mathbf{A}_{k-1} + \mathbf{A}_{k+1} - \mathbf{A}_k\|_F = 0$, where $\mathbf{U}_{k-1} \Sigma_{k-1} \mathbf{V}_{k-1}^\top$ is the SVD of the matrix $\mathbf{X}_k + \rho_{k-1} \mathbf{A}_{k-1}$. \square

References

- [1] A. Buades, B. Coll, and J. M. Morel. A non-local algorithm for image denoising. *IEEE Conference on Computer Vision and Pattern Recognition (CVPR)*, pages 60–65, 2005. 1
- [2] K. Dabov, A. Foi, V. Katkovnik, and K. Egiazarian. Image denoising by sparse 3-D transform-domain collaborative filtering. *IEEE Transactions on Image Processing*, 16(8):2080–2095, 2007. 1, 2, 5, 6, 7, 9
- [3] M. Elad and M. Aharon. Image denoising via sparse and redundant representations over learned dictionaries. *IEEE Transactions on Image Processing*, 15(12):3736–3745, 2006.
- [4] J. Mairal, F. Bach, J. Ponce, G. Sapiro, and A. Zisserman. Non-local sparse models for image restoration. *IEEE International Conference on Computer Vision (ICCV)*, pages 2272–2279, 2009.
- [5] W. Dong, L. Zhang, G. Shi, and X. Li. Nonlocally centralized sparse representation for image restoration. *IEEE Transactions on Image Processing*, 22(4):1620–1630, 2013.
- [6] J. Xu, L. Zhang, W. Zuo, D. Zhang, and X. Feng. Patch group based nonlocal self-similarity prior learning for image denoising. *IEEE International Conference on Computer Vision (ICCV)*, pages 244–252, 2015.
- [7] S. Gu, L. Zhang, W. Zuo, and X. Feng. Weighted nuclear norm minimization with application to image denoising. *IEEE Conference on Computer Vision and Pattern Recognition (CVPR)*, pages 2862–2869, 2014. 1, 2, 5, 6, 7, 9

- 972 [8] S. Roth and M. J. Black. Fields of experts. *International* 1026
973 *Journal of Computer Vision*, 82(2):205–229, 2009. 1 1027
974
- 975 [9] D. Zoran and Y. Weiss. From learning models of natural 1028
976 image patches to whole image restoration. *IEEE International* 1029
977 *Conference on Computer Vision (ICCV)*, pages 479– 1030
978 486, 2011. 2
- 979 [10] H. C. Burger, C. J. Schuler, and S. Harmeling. Image 1031
980 denoising: Can plain neural networks compete with BM3D? 1032
981 *IEEE Conference on Computer Vision and Pattern Recog- 1033
982 nition (CVPR)*, pages 2392–2399, 2012. 5, 6, 7, 9 1034
983
- 984 [11] U. Schmidt and S. Roth. Shrinkage fields for effective 1035
985 image restoration. *IEEE Conference on Computer Vision and 1036
986 Pattern Recognition (CVPR)*, pages 2774–2781, June 2014. 1037
987 5 2
- 988 [12] Y. Chen, W. Yu, and T. Pock. On learning optimized 1038
989 reaction diffusion processes for effective image restoration. 1039
990 *IEEE Conference on Computer Vision and Pattern Recog- 1040
991 nition (CVPR)*, pages 5261–5269, 2015. 1, 5, 6, 7, 9 1041
- 992
- 993 [13] H. C. Karaimer and M. S. Brown. A software platform 1042
994 for manipulating the camera imaging pipeline. *European Con- 1043
995 ference on Computer Vision (ECCV)*, October 2016. 1 1044
- 996 [14] Julien Mairal, Michael Elad, and Guillermo Sapiro. 1045
997 Sparse representation for color image restoration. *IEEE Transac- 1046
998 tions on Image Processing*, 17(1):53–69, 2008. 1, 2 1047
- 999
- 1000 [15] K. Dabov, A. Foi, V. Katkovnik, and K. Egiazarian. 1048
1001 Color image denoising via sparse 3D collaborative filter- 1049
1002 ing with grouping constraint in luminance-chrominance 1050
1003 space. *IEEE International Conference on Image Processing (ICIP)*, 1051
1004 pages 313–316, 2007. 1, 2, 5, 6, 7, 9 1052
- 1005
- 1006 [16] C. Liu, R. Szeliski, S. Bing Kang, C. L. Zitnick, and W. T. 1053
1007 Freeman. Automatic estimation and removal of noise from 1054
1008 a single image. *IEEE Transactions on Pattern Analysis and 1055
1009 Machine Intelligence*, 30(2):299–314, 2008. 1, 2 1056
- 1010
- 1011 [17] M. Lebrun, M. Colom, and J.-M. Morel. Multiscale image 1057
1012 blind denoising. *IEEE Transactions on Image Processing*, 1058
1013 24(10):3149–3161, 2015. 2, 5, 6, 7, 9 1059
- 1014
- 1015 [18] S. Nam, Y. Hwang, Y. Matsushita, and S. J. Kim. A holistic 1060
1016 approach to cross-channel image noise modeling and its ap- 1061
1017 plication to image denoising. *IEEE Conference on Computer 1062
1018 Vision and Pattern Recognition (CVPR)*, pages 1683–1691, 1063
1019 2016. 1, 2, 6, 7, 8, 9 1064
- 1020
- 1021 [19] F. Zhu, G. Chen, and P.-A. Heng. From noise modeling to 1065
1022 blind image denoising. *IEEE Conference on Computer Vi- 1066
1023 sion and Pattern Recognition (CVPR)*, June 2016. 1, 2 1067
- 1024
- 1025 [20] S. Boyd, N. Parikh, E. Chu, B. Peleato, and J. Eckstein. Dis- 1077
1026 tributed optimization and statistical learning via the alternat- 1078
1027 ing direction method of multipliers. *Found. Trends Mach. 1079
Learn.*, 3(1):1–122, January 2011. 1